DAΦNE TECHNICAL NOTE
INFN - LNF, Accelerator Division

Frascati, May 20, 2004
Note: **BM-14**

REPORT ON DAΦNE MD OF 17-18/03/2004

D. Alesini, M.E. Biagini, A. Drago, A. Gallo, S. Guiducci, C. Milardi, M. Preger, A. Stella, C. Vaccarezza, M. Zobov

1. Introduction

During the week of March 15-21, two shifts were devoted to machine development.
The first shift, on March 17, was dedicated to the characterization of wiggler magnets in both rings. The second day shift was mainly devoted to:

1) measurement of the beam lifetime in both rings;
2) bunch length measurements;
3) measurement of the c_{11} coefficient in the e^- ring ;
4) investigation on the e^+ current threshold due to the e-cloud instability.

2. Wiggler measurements

Measurements of tune shift as a function of the beam horizontal position in two wigglers, one in the "long" arc and one in the "short" arc, were performed in both rings (EL2, PL2, ES2, PS2) in order to quantify the nonlinear components of the wiggler magnetic field. For this purpose, a horizontal bump was performed at the wiggler location and the change in energy due to the dispersion at the corrector locations was corrected by moving the RF frequency. The fractional value of the RF frequency as a function of the bump step in mm is shown in Fig. 1.

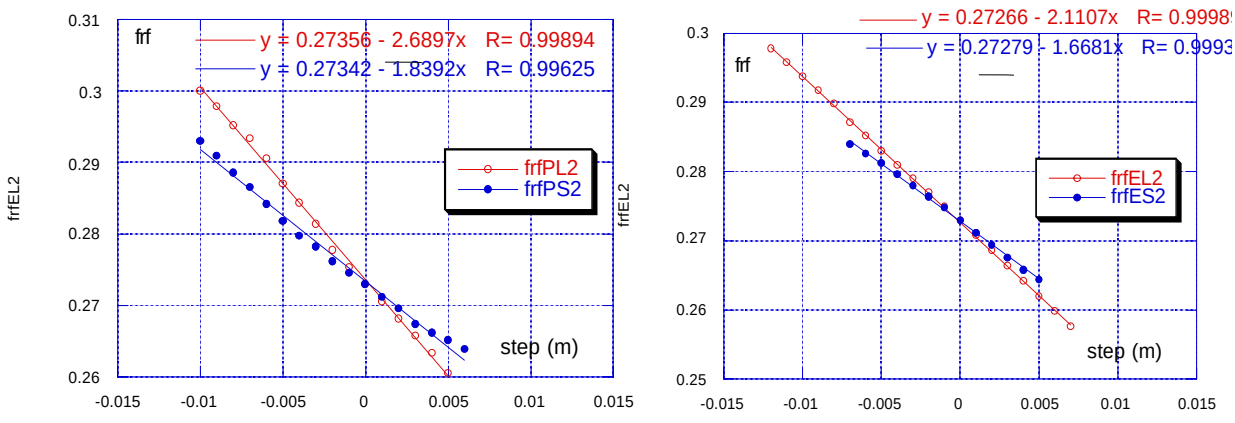

Fig. 1 – Horizontal beam position vs RF frequency for the e^+ (left) and e^- (right) wigglers

To check the linearity of the Beam Position Monitors response, the BPM measured beam position as a function of the bump step in mm has been plotted in Figs. 2 and 3 for electron and positron wigglers respectively.

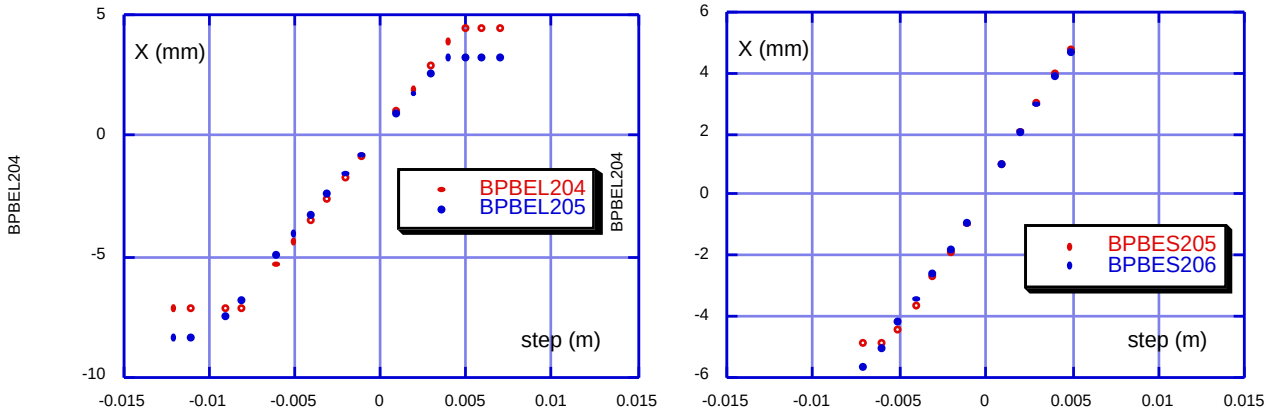

Fig. 2– Bump step vs BPM measured orbit for the e^- wigglers

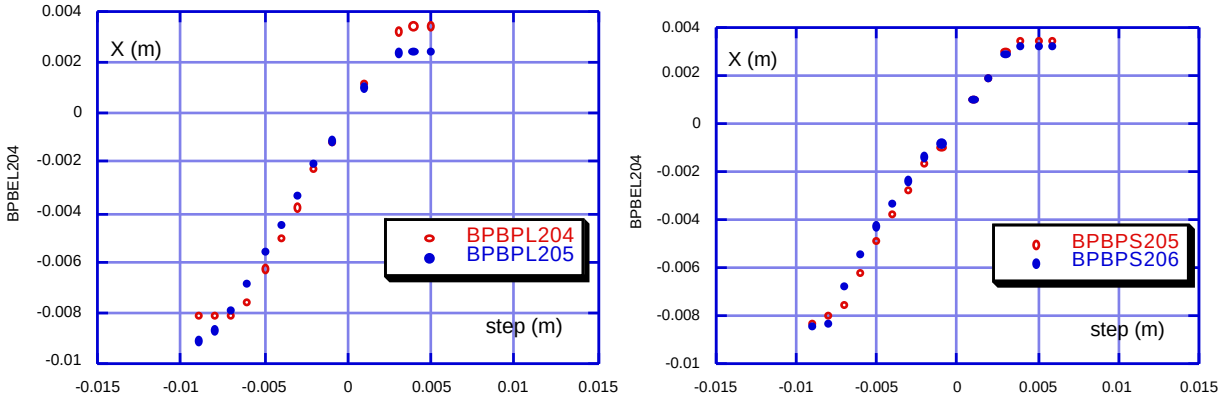

Fig. 3 – Bump step vs measured orbit for the e^+ wigglers

The bump in the behavior of the ES2 wiggler has a much smaller excursion. However for large beam displacements the BPM measured orbit saturates, differently for each wiggler. Those values will not be taken into account when computing the sextupolar and octupolar components of the wiggler fields.

To estimate the non linear components of the wiggler field the tune shift as a function of the orbit amplitude was measured. Figs. 4 and 5 show respectively the horizontal and vertical tunes as measured for the 4 different wigglers as a function of the step in the orbit bump.

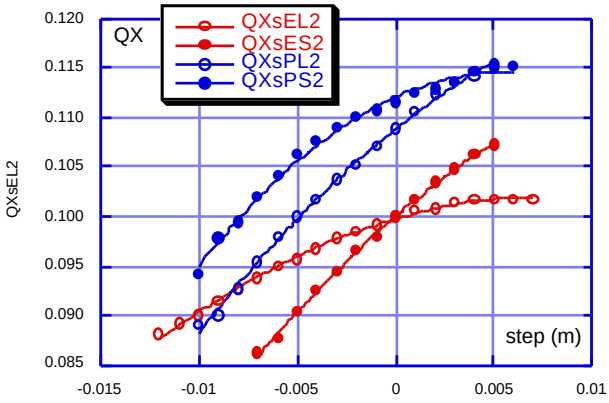

Fig. 4 – Horizontal fractional tune vs horizontal beam displacement

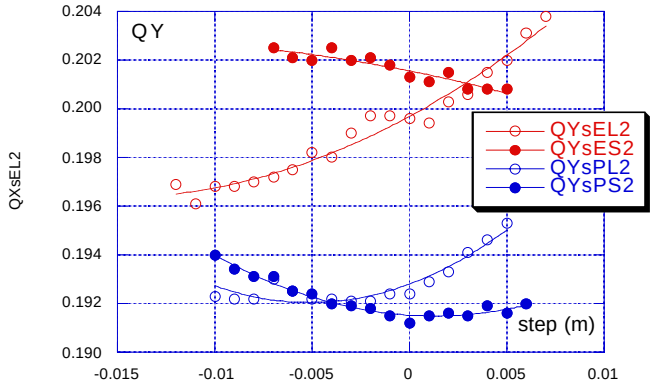

Fig. 5 – Vertical fractional tune vs horizontal beam displacement

To deduce the non linearities we used the horizontal tune shift plotted in Fig. 6, where only measurements in the linear range of the BPMs were taken into account.

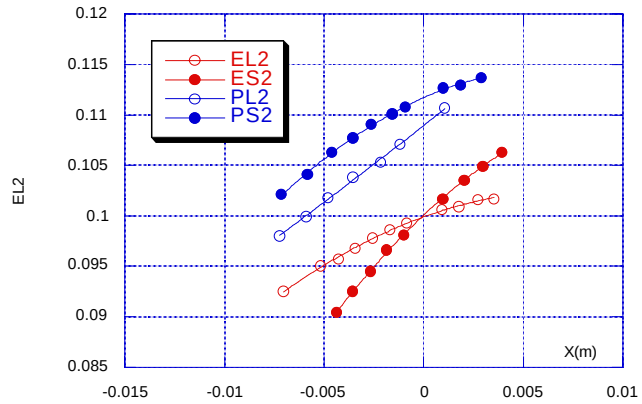

Fig. 6 – Horizontal tune shift vs horizontal BPM reading in the linear range

From a fit of the measured tune it is possible to compute both the sextupolar (m_1) and octupolar (m_2) components:

$$Q = Q_o + m_1 X + m_2 X^2$$

These terms can be introduced in the MAD wiggler model with the following scaling:

$$K_1^{MAD} = \frac{4\pi\, m_1}{\beta}$$

$$K_2^{MAD} = \frac{8\pi\, m_2}{\beta}$$

K_1 being the sextupolar and K_2 the octupolar term. Fig. 7 shows the sextupolar and octupolar terms as computed from the fit (m1-X, m2-X) and from the formulas above. For comparison the same quantities as measured in the 2003 shifts for 2 out of 4 wigglers are reported.

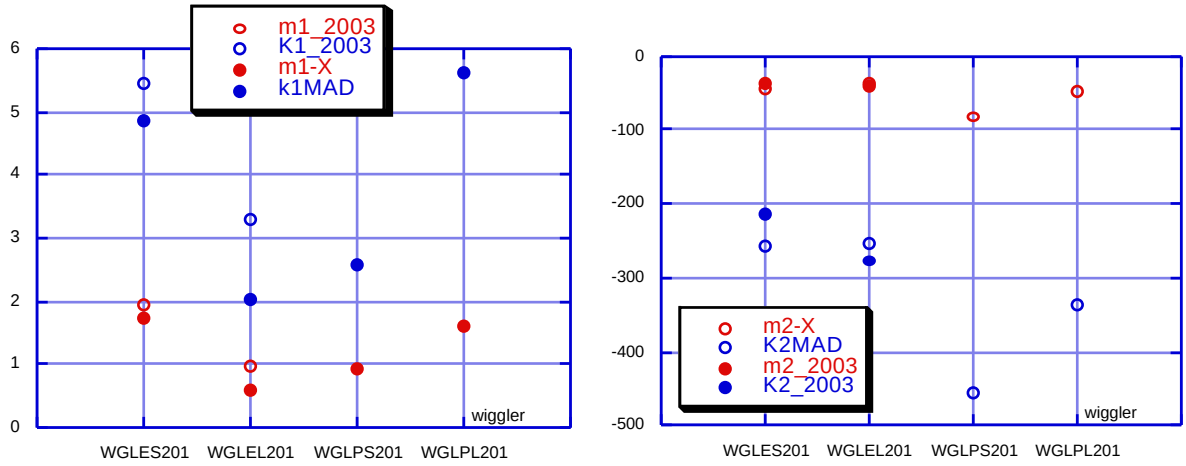

Fig. 7 – Sextupolar (left) and octupolar (right) components

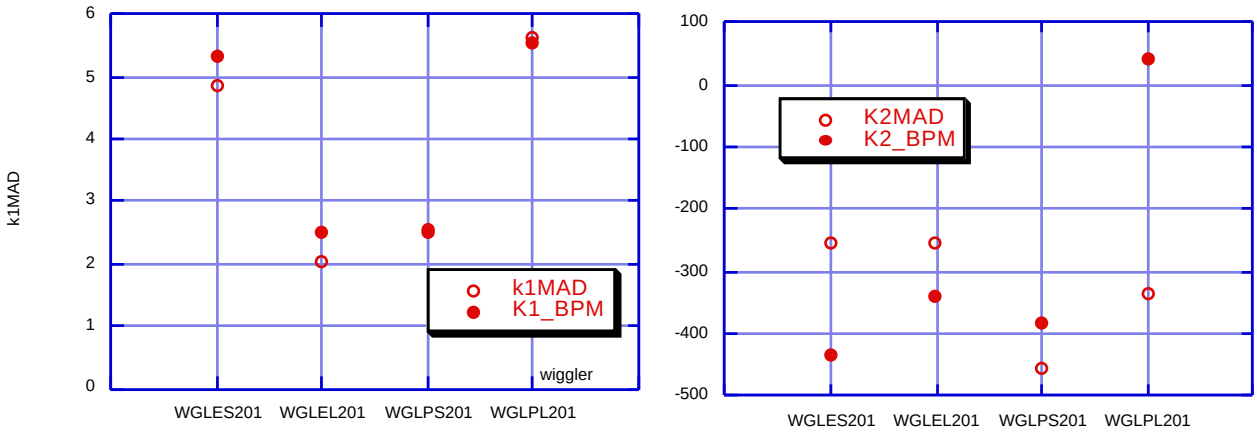

Fig. 8 – Comparison between sextupole (left) and octupole (right) as computed from BPM reading and from bump step

A comparison between the sextupolar and octupolar components as computed by fitting the BPM readings or the bump step value is showed in Fig. 8. While for the sextupole the two values are in good agreement, for the octupole the discrepancy is larger, expecially in wiggler PL2, for which the measured tune shift seems more linear.

As a conclusion we could say that the sextupole term was measured with acceptable error, still being different from wiggler to wiggler, while the octupole term was measured with large uncertainty. The factor 2.5 reduction in the octupolar term predicted by the magnetic measurements seems reasonable.

3. Lifetime measurements

Measurements of the beam lifetime as a function of:

- vertical scraper position
- current
- RF voltage
- beam roundness
- bunch pattern

were performed on both rings.

3.1 Positron ring

The beam lifetime was first measured as a function of the position of the vertical scraper, as shown in Fig. 9. The scraper has two jaws, Up and Down, that were independently moved. The only appreciable decrease in lifetime was observed when the Down jaw was moved beyond 21 mm.

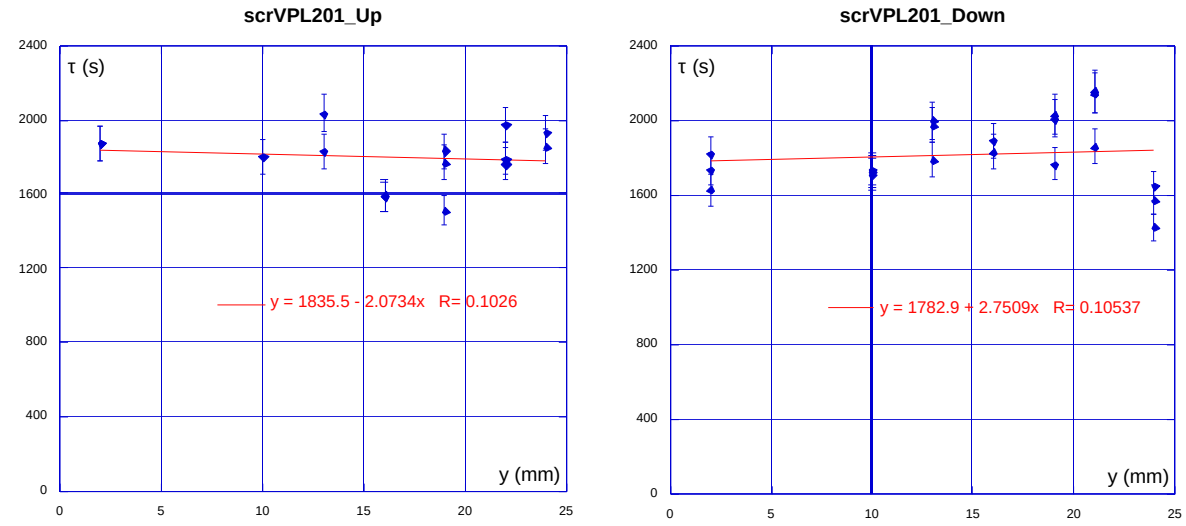

Fig. 9 - Lifetime vs vertical scraper position. Left: Up, right: Down

The beam lifetime was also measured as a function of the beam current, at 180 kV RF voltage (working point). In Fig. 10 the current decay is plotted versus time, together with the beam sizes as measured at the Synchrotron Light Monitor in the same time range. The horizontal beam size is constant, while the vertical decreases with the decreasing current. A good fit to the data is obtained with an exponential curve (solid line) which means that the beam lifetime is constant. This is difficult to explain because for small coupling the beam lifetime in DAΦNE should be dominated by the Touschek effect.

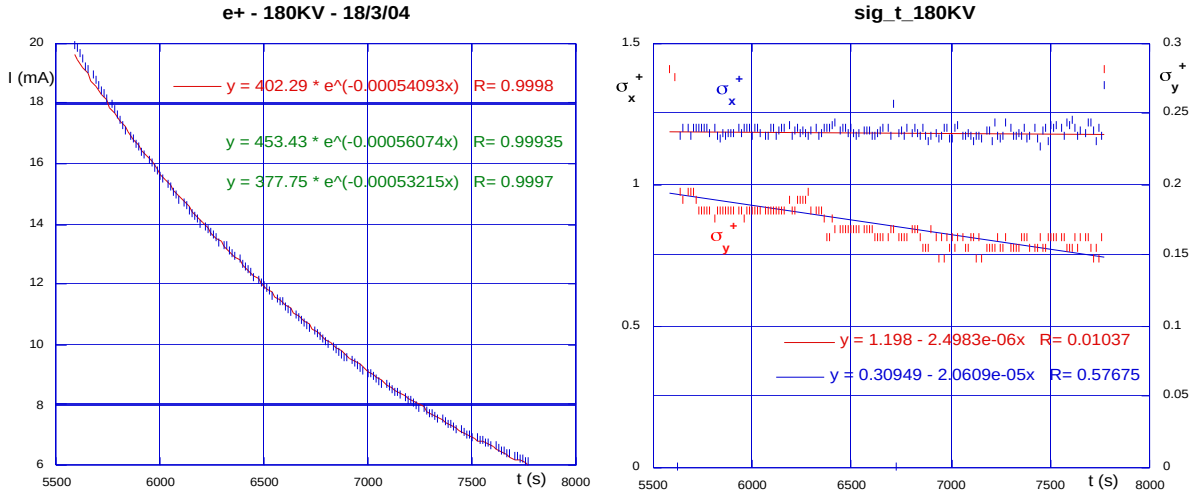

Fig. 10 – Current (left) and beam sizes (right) vs time for Vrf = 180 kV

Neglecting the parameters which are constant in all the measurements below we have:

$$\frac{1}{\tau_{TOU}} \propto \frac{I}{\sqrt{\kappa}\sigma_l \varepsilon_{RF}^2}$$

On the other hand the gas scattering beam lifetime is practically constant because, for single bunch measurements, the pressure rise proportional to the current is negligible with respect to the zero current residual gas pressure.

To investigate on the dependence from the beam roundness ($r=\sigma_y/\sigma_x$), as measured at the SLM, the lifetime as a function of the current in the skew quadrupole PL104 was measured. Fig. 11 shows the behavior of $1/\tau$ as a function of 1/r.

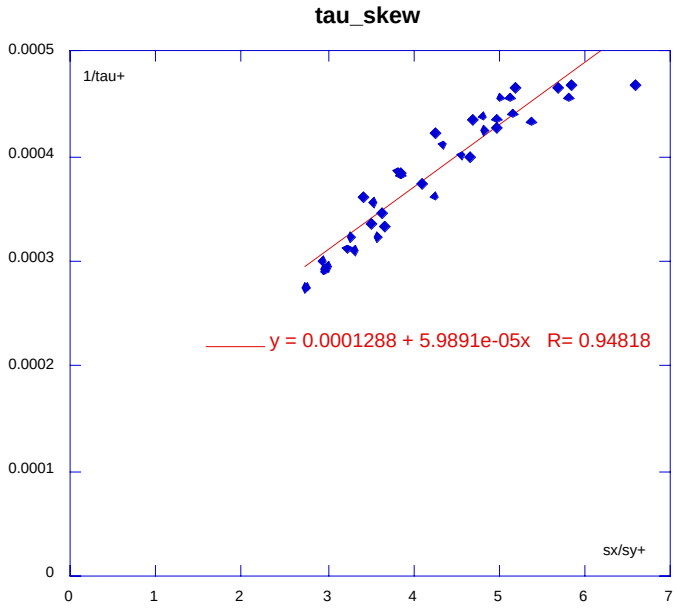

Fig. 11 - Inverse lifetime vs inverse roundess (σ_x/σ_y). Skew PL104

Indeed the linear behavior of the inverse beam lifetime as a function of the inverse roundness is in favour of the assumption that the Touschek effect is the dominant lifetime limitation.

The dependence of σ_y and σ_l on the current (see Fig. 10 and Fig. 18) partially compensates for the variation of $1/\tau_{TOU}$ between 20 and 6 mA, but still the measurements are not completely understood.

The lifetime as a function of the current has been measured as a function of the RF voltage (110, 180 and 250 kV), for the same value of the coupling. It can be seen (Fig. 12, left) that the lifetime increases with the voltage ($V_{RF} \propto \sqrt{\varepsilon_{RF}}$) confirming the fact that the dynamic energy acceptance of the ring is increased with respect to 2002 runs.

The inverse lifetime has also been plotted as a function of current for the three voltages (Fig. 12, right). It can be observed that the higher voltage curves are nearly constant while the 110 KV one has a linear variation with current. In all cases one would expect at zero current a much smaller value of $1/\tau$, corresponding to the inverse of the gas scattering lifetime, being $\tau_{gas} \sim 90000$ sec at $P = 10^{-9}$ Torr.

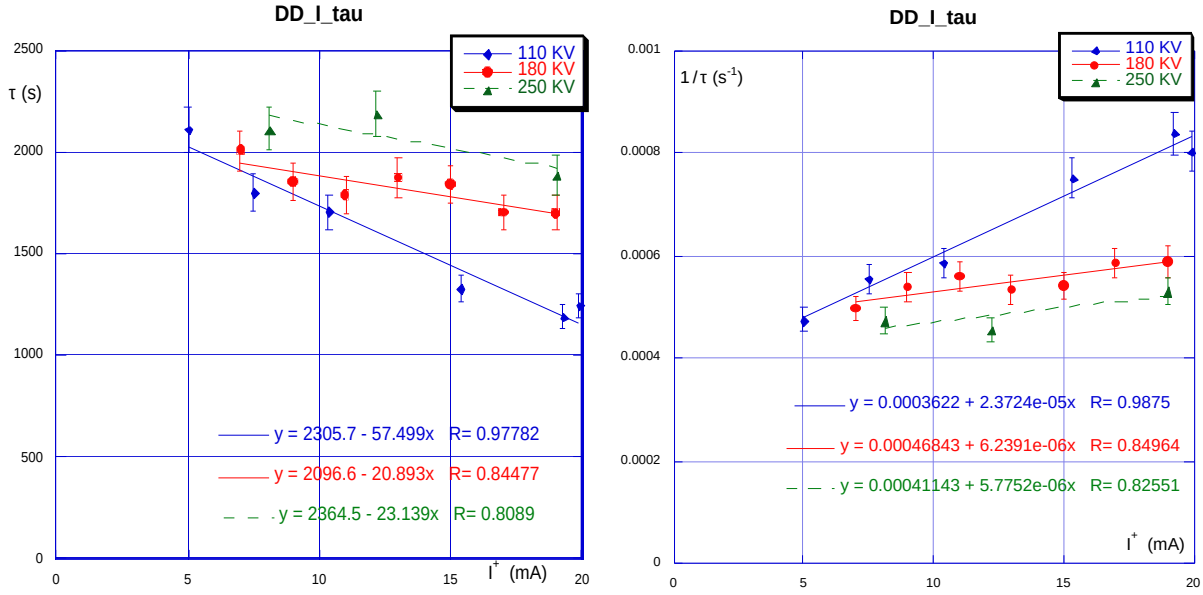

Fig. 12 – Lifetime vs current and inverse lifetime vs current at different RF voltages

A measurement of lifetime at very low current is shown in Fig. 13. At 1.2 mA bunch current the lifetime is 6655 sec, too small compared to the expected gas scattering lifetime. However the error affecting the lifetime measurements has to be accurately computed especially for long lifetimes and small currents.

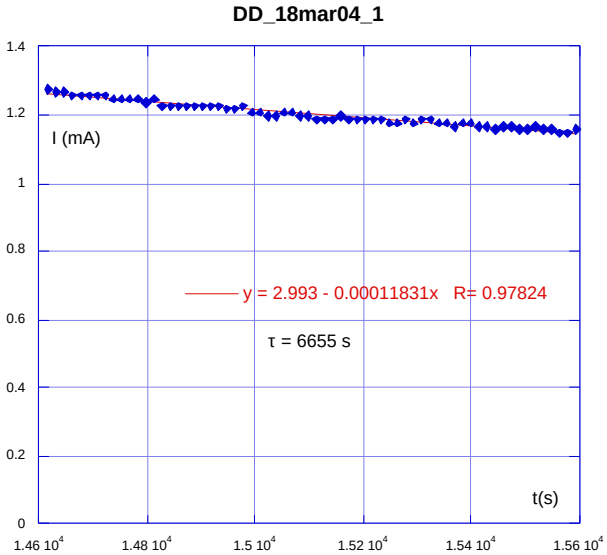

Fig. 13 – Lifetime at low current (1.2 mA)

Finally, a more precise measurement of lifetime for small bunch currents has been done with 100 bunches and it is shown in Fig. 14 (in this case the relative error in the current measurement is smaller). In this case the behavior of 1/τ between 1 and 4 mA/bunch is as expected but between 4 and 6 mA there is a strange effect. It can be noted that near 6 mA/bunch there is the rise up of an instability.

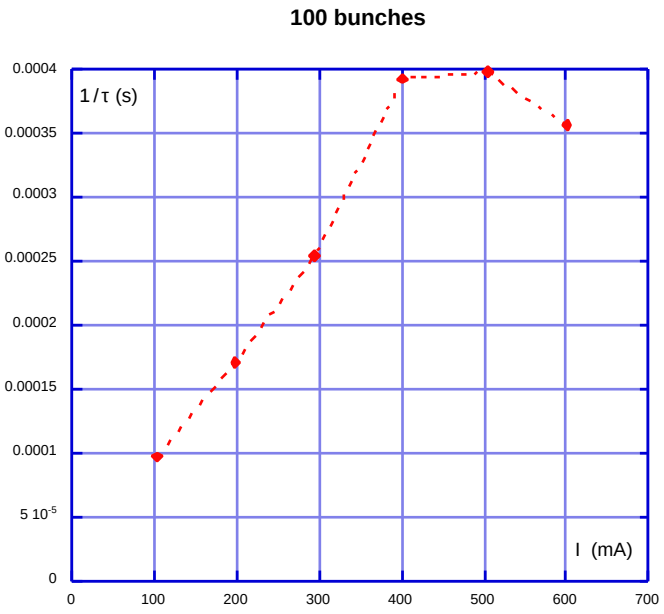

Fig. 14 - Inverse lifetime versus current for 100 bunches pattern

3.2 Electron ring

The same set of measurements was performed on the electron ring and the results are shown in Figs. 15 to 17.

Only one vertical scraper was operating in the e- ring, and as we can see from Fig. 15 there is no effect on the lifetime when moving it for 24 mm towards the beam.

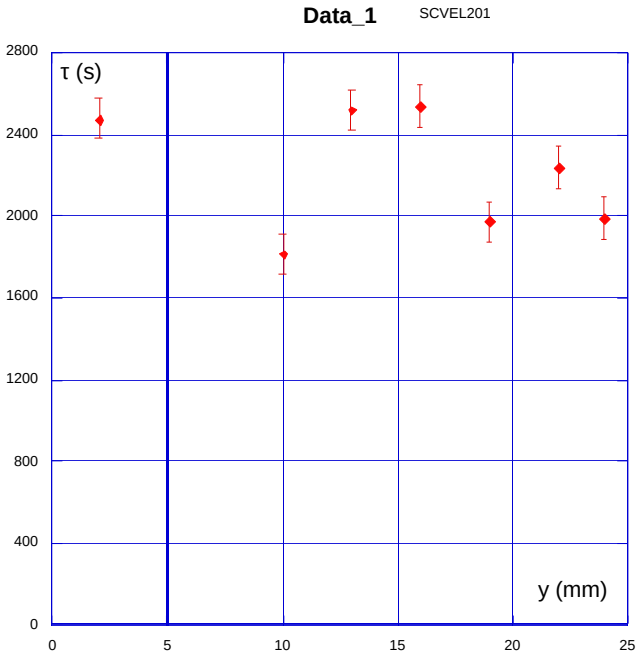

Fig. 15 - Lifetime vs vertical scraper position

The inverse beam lifetime, shown in Fig. 16, is proportional to the inverse roundness as expected for the Touschek effect.

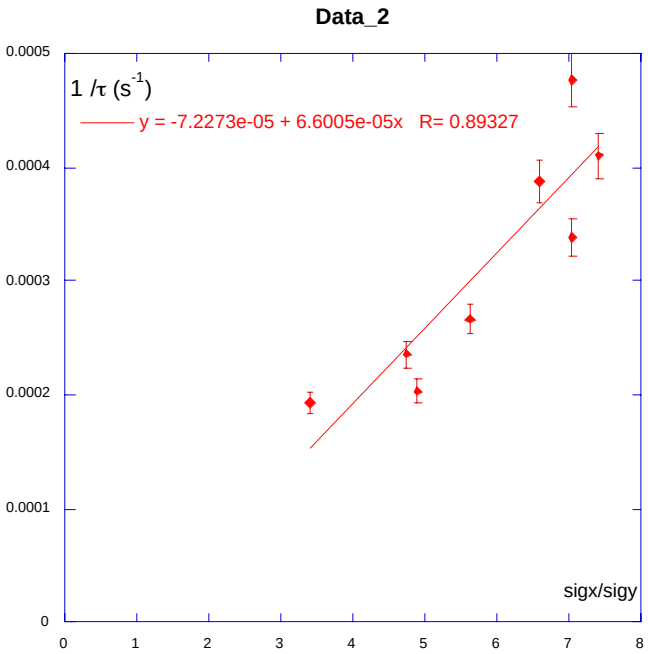

Fig. 16 - Inverse lifetime vs inverse roundness (σ_x/σ_y). Skew ES104

The measurements in Fig. 17 are similar to those shown in Fig. 12 for positrons. The main difference is a strong increase of lifetime with the RF voltage, but this is probably not significant since the vertical beam size was not constant (and unfortunately it was not recorded) during the measurement.

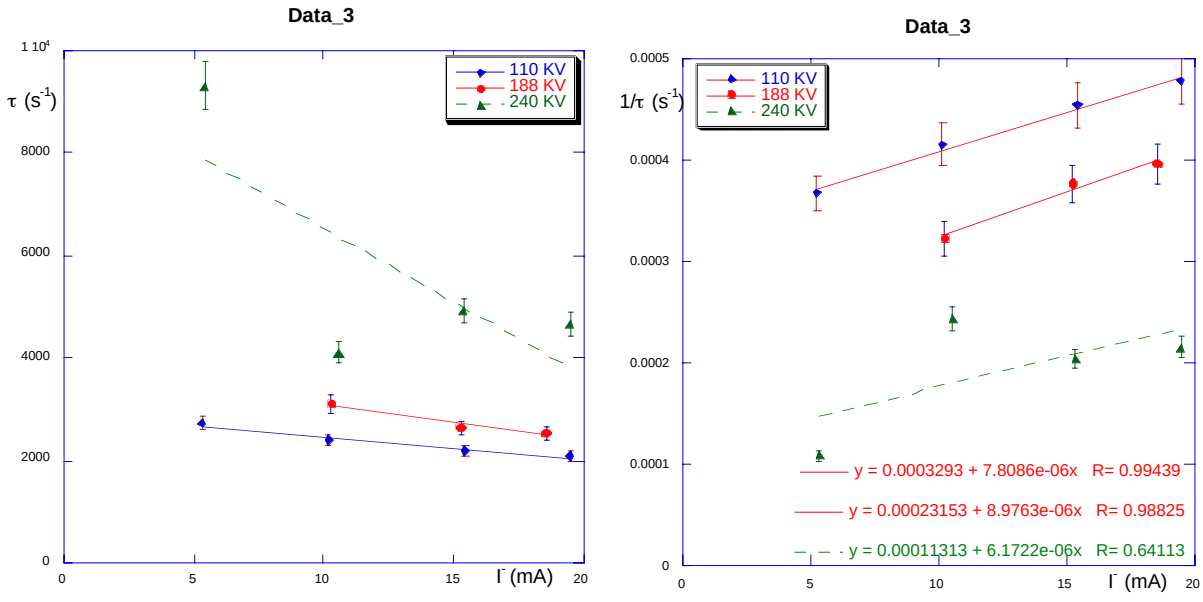

Fig. 17 - Lifetime and 1/τ vs beam current at different RF voltages

4. Bunch length measurements

The bunch length was measured for both beams at different RF voltages (110, 180, 250 kV) as a function of the beam current. Fig. 18 shows the measurements for the e^+ and e^- beams. There is an unexpected bump at 180 kV in the measured bunch length for e^+ around 10 mA.

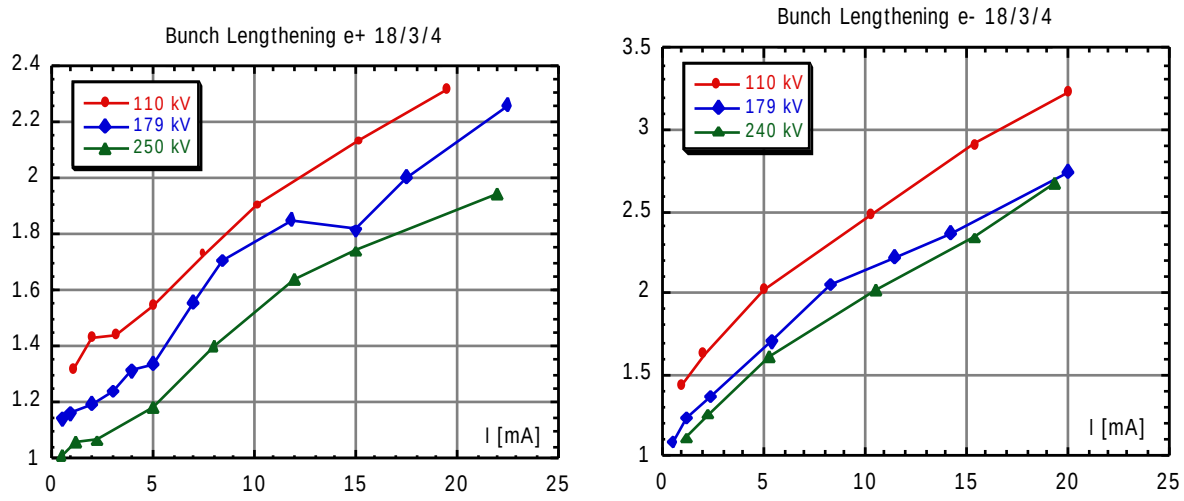

Fig. 18 – Bunch length versus bunch current for different RF voltages: e^+ (left), e^- (right)

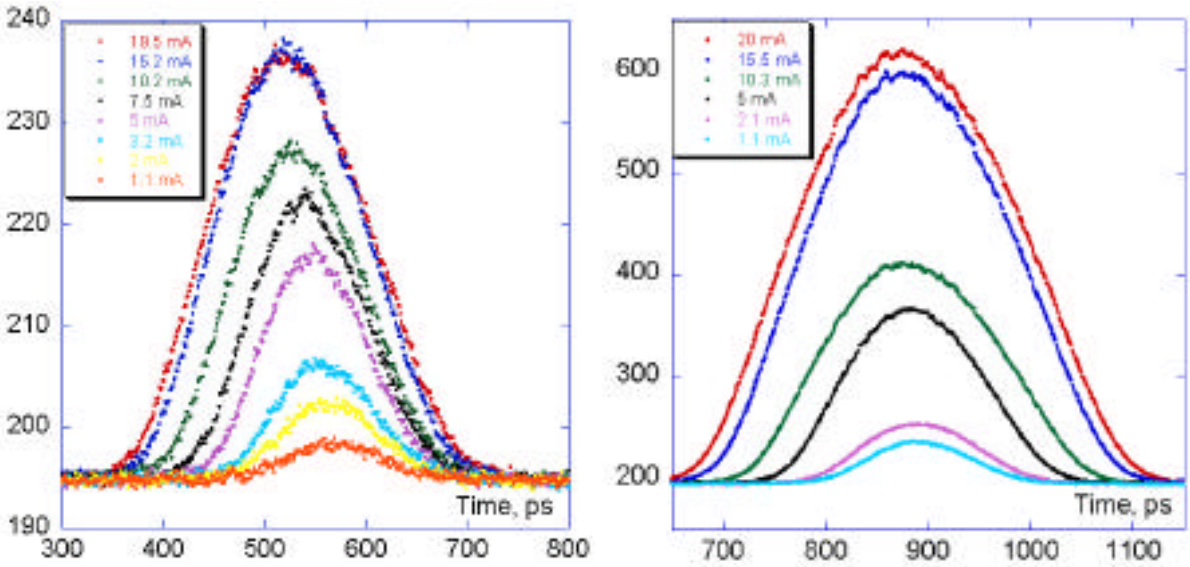

Fig. 19 – Bunch distribution for different bunch currents for e^-(right) and e^+(left)

The bunch distribution for different bunch currents for the two rings is plotted in Fig. 19. Simulations on bunch lengthening were performed in 1998. A comparison between simulations and measurements as a function of the bunch current is presented in Fig. 20. The agreement is satisfactory.

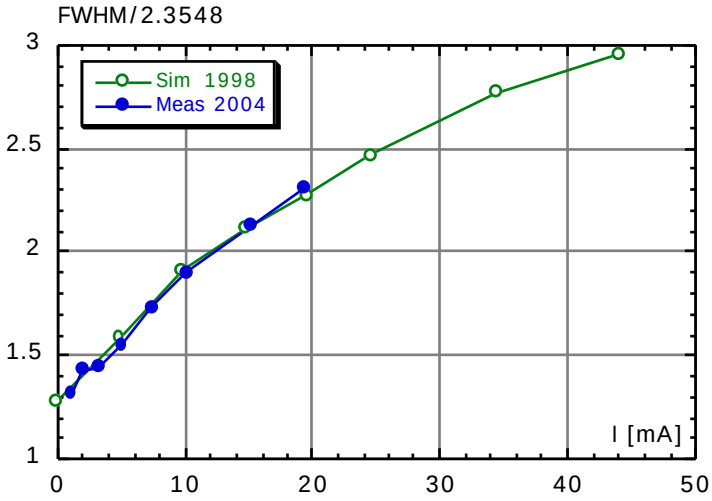

Fig. 20 – Comparison between bunch lengthening simulations and measurements

The bunch length measurements were also repeated with all the scrapers OUT, to check possible effect of the scrapers insertion on the pipe impedance. The comparison between normal operation at 179 kV and scrapers OUT is shown in Fig. 21 for the two rings. The bump is less pronounced but this can be due to the larger measurement interval.

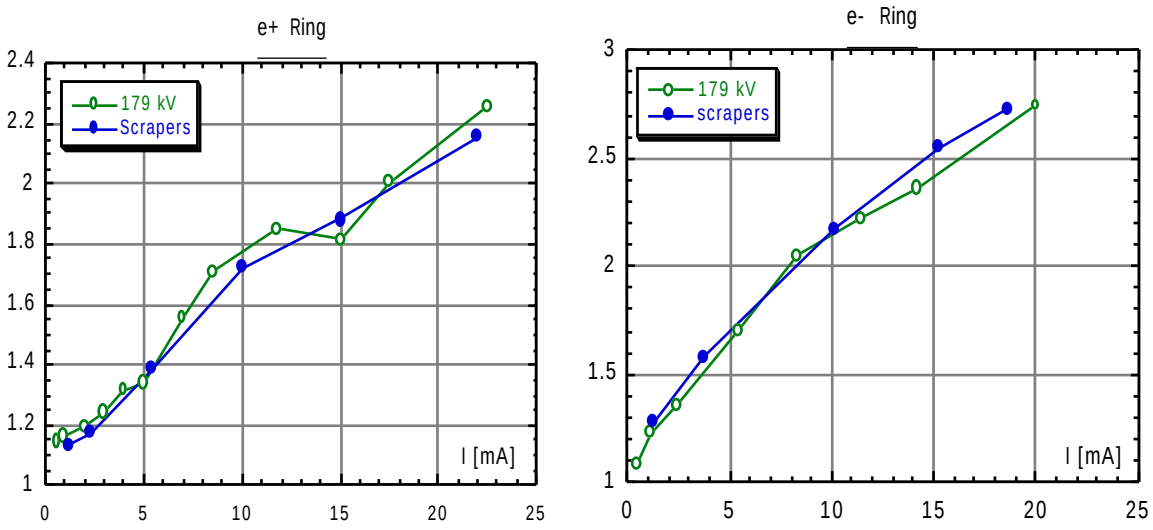

Fig. 21 – Bunch lengthening scrapers OFF and ON for e^-(right) and e^+(left)

5. Beam decoherence measurement

Measurements of the beam decoherence for the electron ring were also performed. Figure 22 shows the beam oscillation due to a horizontal kick, by one of the injection kickers, as a function of the number of turns, for two different kick amplitudes. The kicker delay was adjusted when very low voltages were applied. The value of the c_{11} coefficient is derived from a fit of the oscillation amplitude; both measurements give about the same c_{11} value.

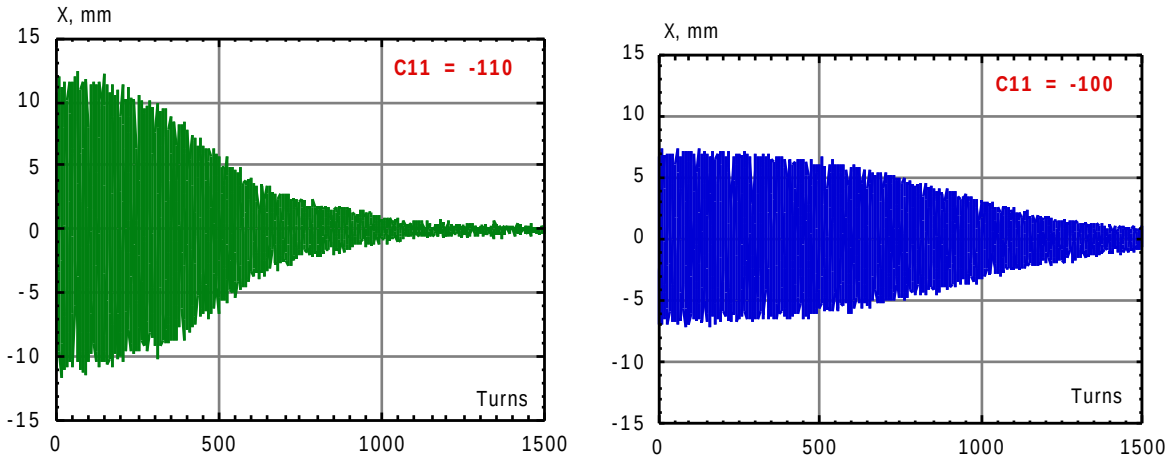

Fig. 22 – e^- beam decoherence forVkick=4 kV (right) and 8 kV (left)

The performed measurements are summarized in Table I. The measurements in the standard operation configuration are all compatible with a c_{11} value around -100. When the sextupoles are ramped down to 60% of their standard settings the non linearity clearly shows up, the conclusion being that the present sextupoles setting is able to control the octupolar terms present in the electron ring.

Table I – Summary of beam decoherence measurements

V [kV]	I[mA]	Δx [mm]	Turns	ΔQ_x	c_{11}	Comments
3	1.84	3.8723	1870	0.10427	-105	
4	1.79	4.3393	1693	0.10423	-104	
5	1.74	4.1865	1735	0.10422	-105	R = 0.99975
6	1.74	3.7903	1871	0.10426	-107	
8	1.71	2.6951	2339	0.10434	-121	$X \sim \sigma_x$
4	1.61	4.4428	1671	0.10424	-102	
5	1.38	7.4357	1071	0.10419	-96	+58 nsec
8	1.23	11.953	575	0.10373	-111	+98 nsec
2	.9	0.9863	258	0.10161	-2990	Sext 60%, $X < \sigma_x$
3	.7	1.8399	443	0.1036	-934	Sext 60%, $X \sim \sigma_x$
4	.6	3.1293	262	0.10193	-928	Sext 60%
8	.5	5.2282	128	0.09947	-1137	Resonance Beating

6. e^- cloud measurements

Measurements to start investigation on the presence of the e^- cloud instability in the positron ring were performed. In positron storage rings electrons produced by photoemission, ionization and secondary emission accumulate in the vacuum chamber and form an “electron cloud” which can reach high charge density for some beam operation modes. The response of this electron cloud to a transversely displaced bunch resembles a short–range wakefield and can cause a fast instability. In addition, beam-induced multipacting of the electrons may lead to an enhanced gas desorption and an associate pressure increase.

In particular were measured:

a) the correlation between the total positron current and a straight section Vacuum Gauge reading, with different bunch patterns and transverse feedback ON and OFF;
b) the transverse bunch size at SLM as a function of total positron current (with different patterns and transverse feedback ON and OFF);
c) the correlation between tune shift and total positron current (with different patterns and transverse feedback ON and OFF).

The VGPL03 reading and the positron beam current for different bunch patterns (90 bunches-mod.1, 45 bunches-mod.2), with transverse feedback ON and OFF, are shown in Fig. 23.

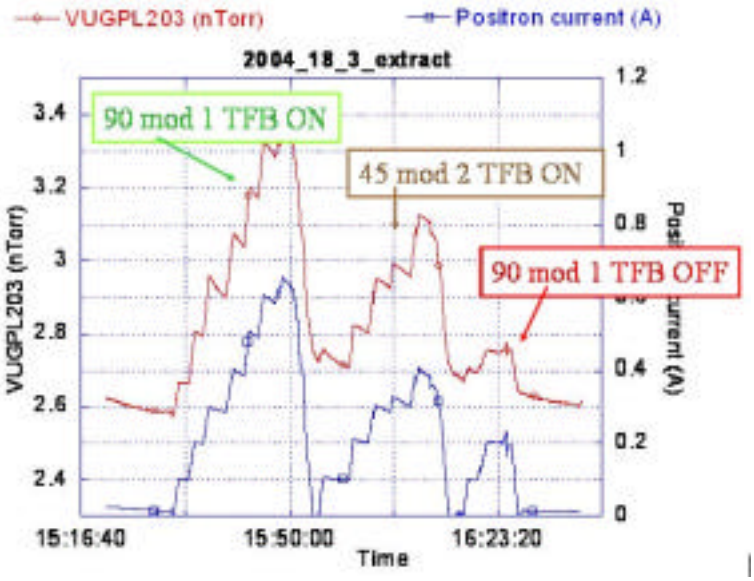

Fig. 23 – e^+ ring: VGPL03 readings(red) and positron beam current (blue) for different bunch patterns

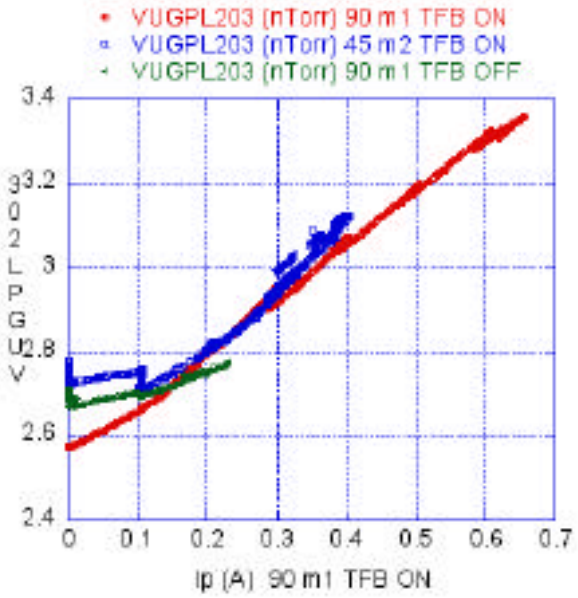

Fig. 24 – e^+ ring: VGPL03 readings vs beam current for different bunch patterns: 90-mod.1-TFB ON (red), 90-mod.1-TFB OFF (green), 45-mod.2-TFB ON (blue)

Fig. 24 shows a comparison of the VGPL03 readings for the different bunch patterns as a function of the beam current in the 90 bunches-mod.1 pattern.

A comparison of the horizontal and vertical beam sizes as measured at the SLM, for the same 3 bunch patterns, is plotted in Fig. 25, and the correlation between vacuum readings and beam current in Fig. 26.

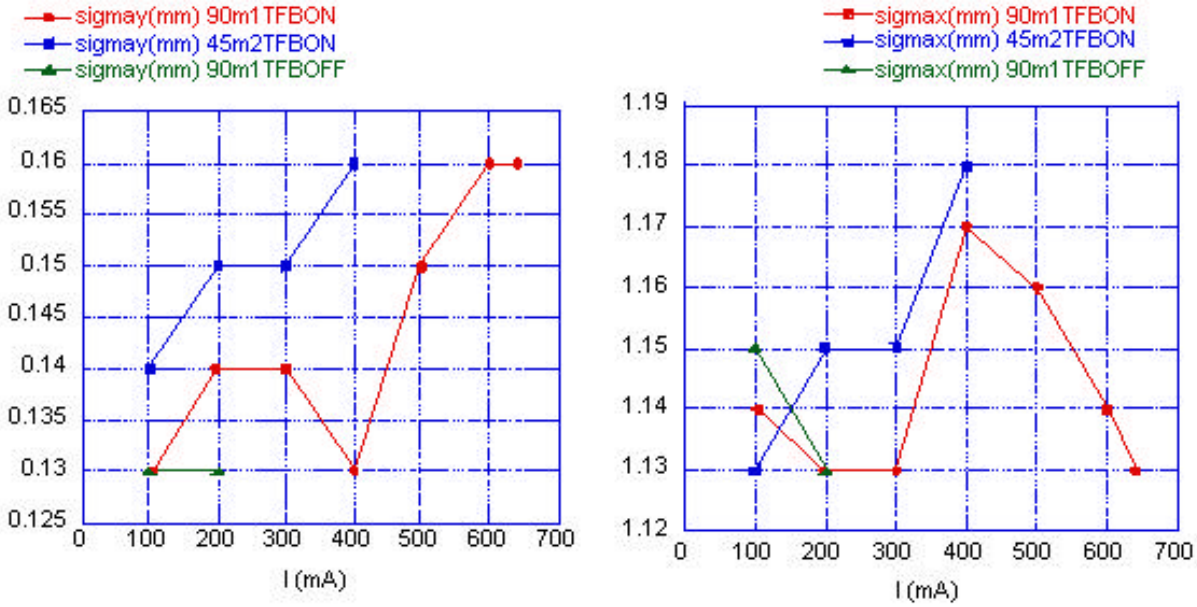

Fig. 25 – Horizontal (left) vertical(right) beam size for different bunch patterns: 90-mod.1-TFB ON (red), 90-mod.1-TFB OFF (green), 45-mod.2-TFB ON (blue)

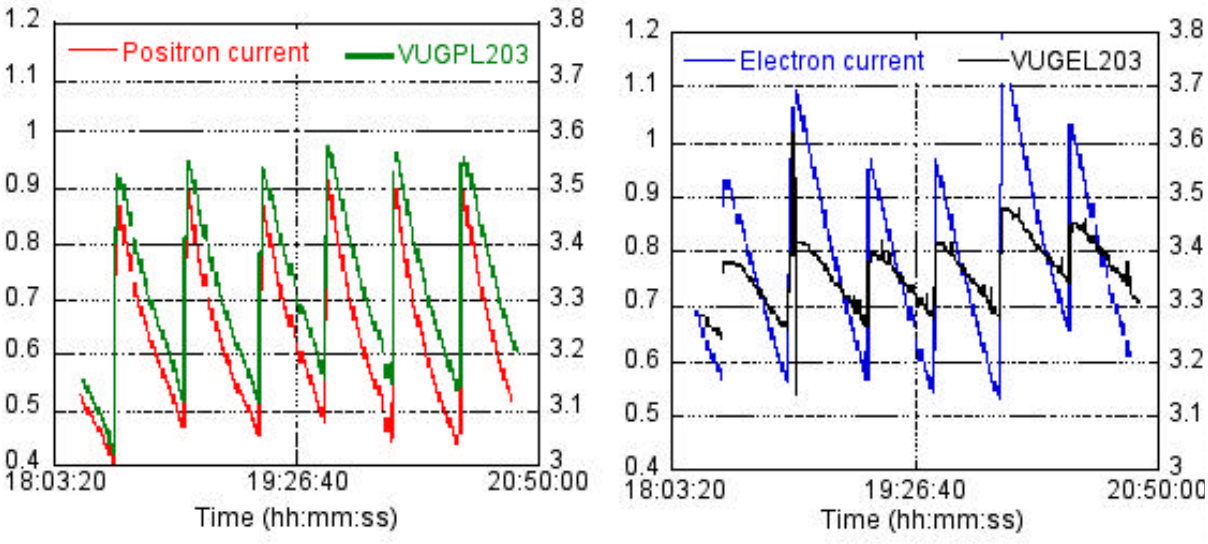

Fig. 26 – Correlation between current and VG readings for e^+ (left) and e^- (right)

The tune shifts versus current for the three sets of measurements are plotted in Fig. 27. For comparison, in Fig. 28 are reported the positron tune shifts (left) and the electron ones (right), previously measured, on the same scale. The difference in the Q_x behavior is striking.

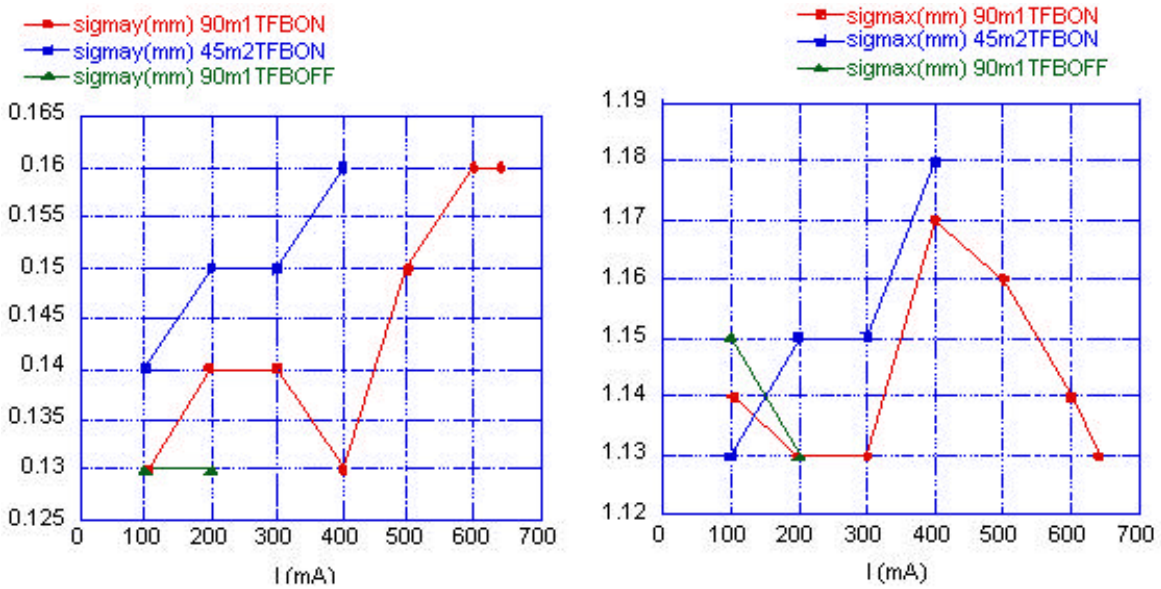

Fig. 27 – Horizontal (left) and vertical (right) tunes for different bunch patterns: 90-mod.1-TFB ON (red), 90-mod.1-TFB OFF (green), 45-mod.2-TFB ON (blue)

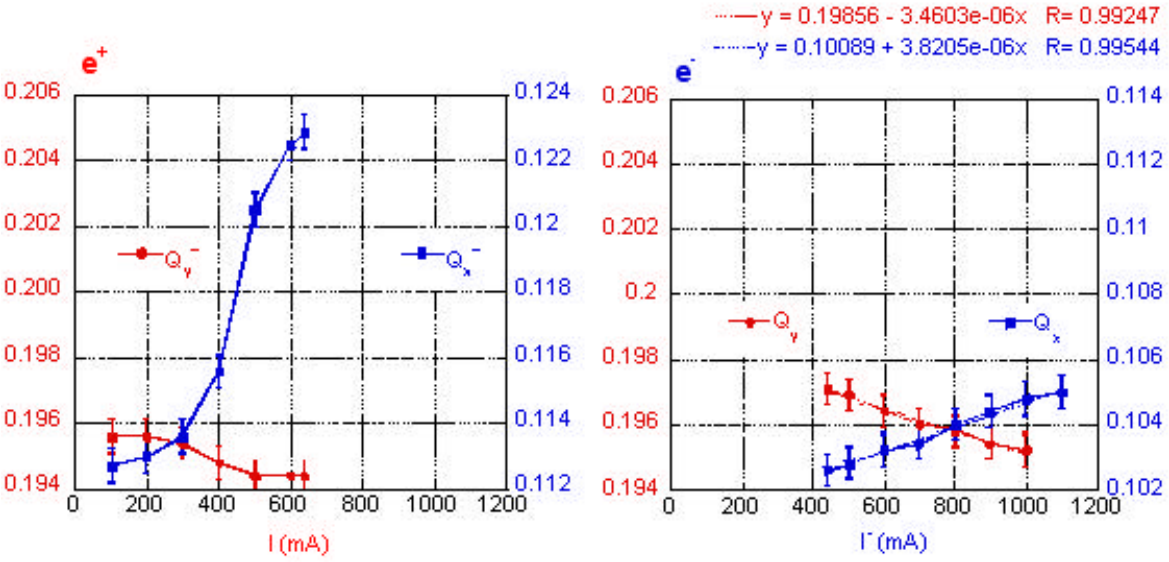

Fig. 28 – Positron (left) and electron (right) tune shifst vs current

The injection current threshold as measured in different bunch patterns and transverse feedback setting is reported in Table II. The last row is a measurement of the threshold performed in 2002 with the KLOE configuration.

Table II – Injection current threshold

Pattern	**TFB**	**Spacing(m)**	**I_{max} (mA)**
90/120	ON	0.8	650
45/60	ON	1.6	400
90/120	OFF	0.8	200
30/120+gap+30/120+gap	ON	0.8	600
90/120 with e^- beam	ON	0.8	900
45/120 KLOE conf.	ON	1.6	1300

As preliminary conclusions we can summarize some of the hints that the e-cloud instability could be present:

- the growth of beam sizes without the TFB;
- the different behaviour of the current induced tune shift for e^+/e^-;
- there are few betatron sidebands: the tune is split in two or more lines;
- the slight beam size increase with current.

On the other side there are other observations against this hypothesis, like:

- a single bunch instability at I ≥15mA (horizontal plane);
- the single bunch beam size increase;
- the current threshold in the 90/120 bunch pattern is smaller by a factor 2 than in 45/60;
- there is no evident multipacting induced vacuum increase at the threshold.